Aeroacoustic simulation of a flow-excited Helmholtz resonator using OpenFOAM

Péter Rucz[1]

[1] *Budapest University of Technology and Economics, Budapest, Hungary, Email: rucz@hit.bme.hu*

Introduction

The flow-excited Helmholtz resonator is a classical example of acoustical resonance induced by fluid flow. Similar phenomena of sound production are also responsible for the noise amplification in ventilation ducts with side branches and the sound generation of air reed wind instruments, for example. In the past few years several studies investigating the fluid flow and the acoustical feedback in the Helmholtz resonator were published. These examinations include analytical treatments, experiments, and simulations based on discrete vortex dynamic models and computational fluid dynamics.

This paper presents the aeroacoustic simulation of a Helmholtz resonator excited by grazing flow. Numerical computations at different flow speeds are performed by solving the compressible Navier–Stokes equations using the finite volume method implemented in the OpenFOAM software package. First, shear layer oscillations are examined without acoustical feedback in order to determine the frequency of the hydrodynamic modes and to estimate the convection speed of perturbations. Then, the acoustical response of the resonator is computed and the natural frequency and quality factor of the resonator are determined. Finally, flow-induced resonance is simulated at different flow speeds and the results are compared with that of other models published previously.

Problem description

The examined geometry is depicted in Figure 1. The configuration consists of a rectangular wind channel and a box-shaped resonator that is attached to the bottom of the channel. The two parts are connected by a square orifice that functions as the neck of the resonator.

The same configuration were used in the measurements of Ma *et al.* [1], the discrete vortex model (DVM) of Dai *et al.* [2], and the 3D LES study by Ghanadi *et al.* [3]. The only difference in the geometry in these works is the edge of the resonator: in the measurements a sharp edge with 30° was set, in the DVM the thickness of the plate is neglected, and in the 3D simulations blunt 90° edges were modeled. Here, the latter variant is examined.

In the present study a 2D model of the longitudinal section of the geometry shown in Figure 1 is created. The structured mesh contains a single layer of hexahedral elements. The minimum edge size, used at the leading and trailing edges of the orifice, is 0.2 mm and the maximum edge length is 10 mm. Transition in element size is made such that the coordinate-wise edge lengths of two adjacent elements differ up to a maximum of 5%. This resulted in a mesh having ≈ 85 000 elements.

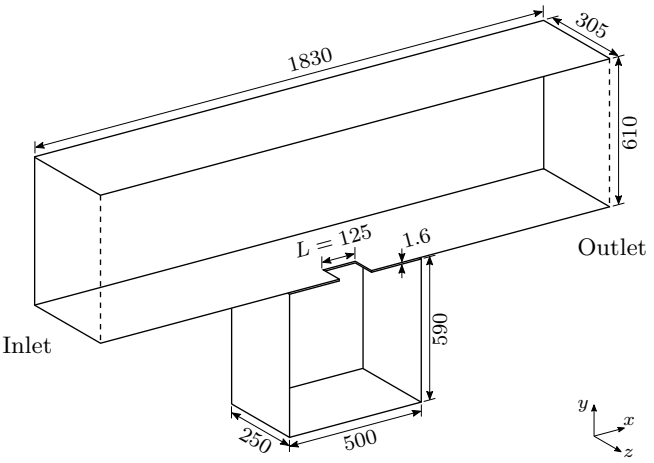

Figure 1: Geometry of the simulated Helmholtz resonator and wind channel. All sizes are given in mm units.

At the inlet a time varying velocity is set, that smoothly increases to the final freestream velocity U in 0.25 s using a raised cosine function. The top wall is assumed to be frictionless and a slip boundary condition is used there, while at other walls no-slip is prescribed. The k–ω SST turbulence model is applied in both incompressible and compressible simulations. This choice is justified by the relatively high Reynolds numbers $\mathrm{Re} \approx 2 \cdot 10^5 \ldots 1.5 \cdot 10^6$ and the resolution of the mesh that gave non-dimensional wall distances at the bottom plane of the wind channel in the range $y^+ \approx 0.5 \ldots 10$, depending on the freestream velocity U. Postprocessing is facilitated by using several pressure probes inside the resonator and the channel and a number of velocity probes across the orifice. All simulations were carried out using `OpenFOAM-v1812` [4].

Shear layer oscillations

When the resonator is excited by grazing flow, there is a large difference of streamwise velocity above and below the orifice of the resonator. Thus, at the orifice an unstable shear layer develops that is capable of hydrodynamic oscillations even without acoustical feedback. First, these oscillations are investigated at different flow speeds. To eliminate the acoustical effect of the resonator, incompressible flow conditions are assumed.

The frequency of shear layer oscillations can be predicted using Rossiter's general formula that estimates the frequency of the n-th hydrodynamic mode f_n as

$$\frac{f_n L}{U} = \frac{n - \alpha}{\mathrm{Ma} + 1/\kappa}, \tag{1}$$

where U is the freestream velocity and $L = 125\,\mathrm{mm}$ is

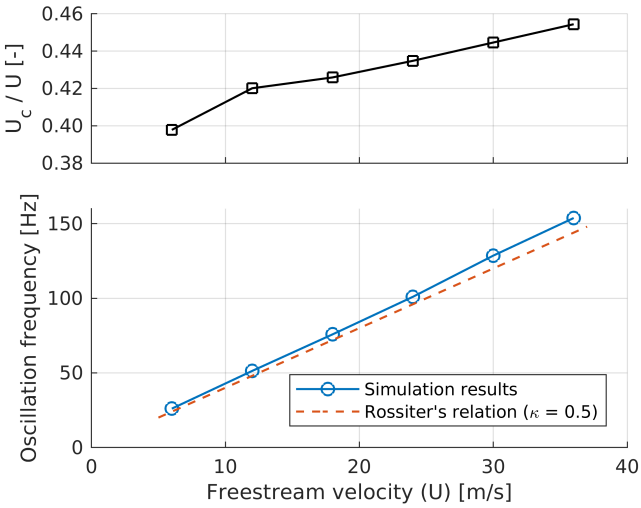

Figure 2: Estimated convection speed (top) and oscillation frequency (bottom) of the first hydrodynamic mode of the shear layer.

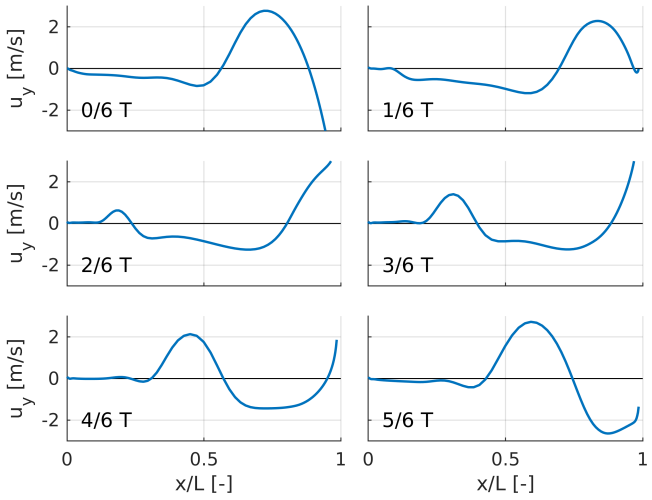

Figure 3: One period of the cross-stream velocity in the shear layer without acoustical feedback at $U = 18\,\mathrm{m/s}$.

the length of the orifice. The constant α is related to the phase delay of the hydrodynamical or acoustical feedback, while $\kappa = U_c/U$ is the ratio of the convection velocity of disturbances inside the shear layer U_c and the freestream velocity. Following [1] $\alpha = 0$ is assumed.

The simulated oscillation frequencies of the first mode ($n = 1$) are compared to the predictions by (1) using $\kappa = 0.5$ in Figure 2. The convection speed of the perturbations can also be estimated using the velocity probe data by averaging the streamwise velocity component u_x over the orifice through one period T of the oscillation:

$$U_c \approx \frac{1}{LT} \int_0^T \int_0^L u_x(x,t)\,\mathrm{d}x\,\mathrm{d}t. \qquad (2)$$

The top diagram of Fig. 2 shows the relative convective speeds estimated using (2). As seen U_c/U slowly increases with the freestream velocity, which can be attributed to the decreasing boundary layer thickness.

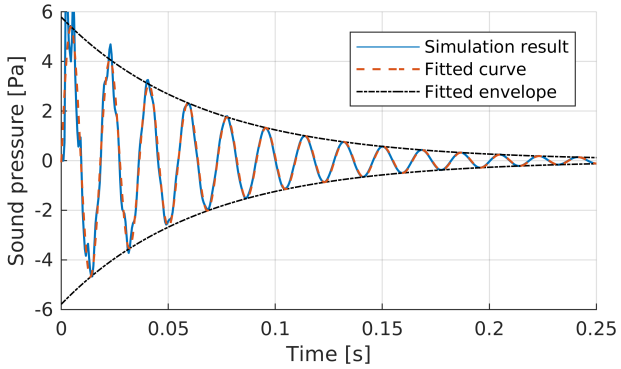

Figure 4: Result of the impulse response simulation using the plenum pressure boundary conditions.

As it is seen, the estimate for $\kappa = U_c/U$ using (2) leads to somewhat lower values than the best fit for the simulated oscillation frequencies. The drawback of the estimation (2) is that it can only estimate the convection speed along a single straight section at $y = 0$, i.e., the top plane of the orifice.

In [1] two alternative methods for estimating U_c from PIV measurements were also introduced. It was found that estimating the convection speed of the vorticity as a whole gives $U_c/U \approx 0.5$, independent of U, while the estimated convection speed of a single vortex can be significantly lower, especially in the case of strong acoustical feedback. However, the convection speed of perturbations without acosutical coupling was not examined.

Figure 3 shows snapshots of the cross-stream velocity over the orifice during one period of the oscillation. The propagation and growth of the disturbance inside the shear layer can clearly be observed. At the trailing edge of the resonator large velocity gradient is observed. Similar behavior was found at all examined flow velocities.

The acoustical response of the resonator

In order to examine the acoustical properties of the resonator, its impulse response was determined using the flow simulation framework. In this case the bottom resonator wall became the inlet of the system, while the two ends of the simulated channel both became outlets, where wave transmissive boundary conditions are applied. At the inlet a plenum pressure boundary condition was prescribed which creates a zero-dimensional model of an enclosed volume of gas upstream of the inlet. The pressure that the boundary condition exerts on the inlet boundary is dependent on the thermodynamic state of the upstream volume. The upstream plenum density and temperature are time-stepped along with the rest of the simulation, and momentum is neglected [4]. The response of the resonator is recorded by the pressure probe located at the middle of the orifice. Impulse response simulations were performed without using turbulence models.

The simulated acoustical response of the resonator is displayed in Figure 4. As it is seen, after some irregularities in the initial phase ($t < 0.1$) an oscillating and exponen-

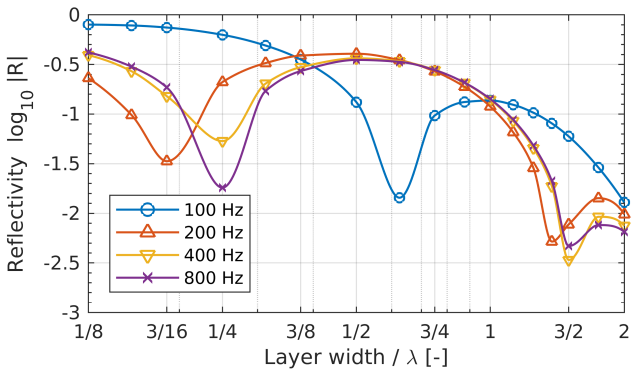

Figure 5: Reflectivity of the acoustical damping layer at different frequencies and layer widths.

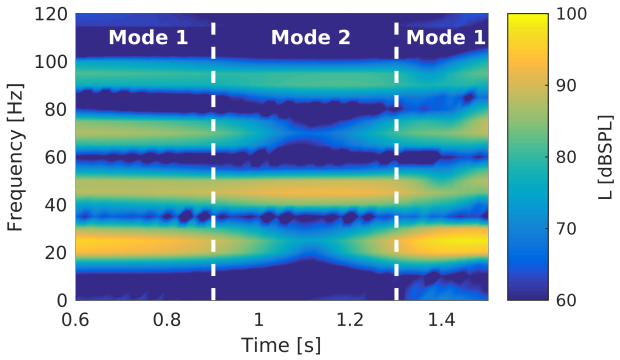

Figure 6: Spectrogram of the fluctuating pressure at the bottom center position of the resonator with $U = 6\,\mathrm{m/s}$.

tially decaying response is attained. The frequency f_{hr} and the quality factor Q of the natural resonance was determined by means of a complex exponential fit. The fit resulted in $f_{\mathrm{hr}} = 54.8\,\mathrm{Hz}$ and $Q = 11.8$, which is in good agreement with the measurement results ($f_{\mathrm{meas}} = 46\,\mathrm{Hz}$ and $Q_{\mathrm{meas}} = 11$) given in [1]. It must be noted, however, that some discrepancies should be expected because of the 2D model used here.

Acoustical damping layer

In the first compressible simulation attempts a parasite effect was observed, namely, a strong harmonic peak with $f \approx 90\,\mathrm{Hz}$ occurred independent of the freestream flow velocity. By examining pressure probe data, it was found that this effect was due to the reflections from the inlet; the upstream section of the channel functioned as a quarter-wavelength resonator. The same behavior was observed with changing the length of the upstream channel section.

To reduce the effect of spurious reflections of acoustical waves from the boundaries, an acoustical damping layer (often referred to as sponge layer) was utilized. Inside the sponge layer the governing equations are modified by introducing artificial dissipation terms following [5, chapter 5] as

$$\frac{\partial \mathbf{u}}{\partial t} = \mathcal{L}(\mathbf{u}) - \nu\,(\mathbf{u} - \mathbf{u}_{\mathrm{ref}})\,, \tag{3}$$

where $\mathbf{u}$ is the solution vector, $\mathcal{L}$ represents the spatial operators acting on $\mathbf{u}$, and $\mathbf{u}_{\mathrm{ref}}$ is the reference field, which is calculated as the time average of the simulated solution. The damping factor ν is smoothly increased inside the layer using a raised cosine function

$$\nu = \nu_{\max} \frac{1 - \cos(\pi d/W)}{2}, \tag{4}$$

with d denoting the depth inside the layer ($0 \le d \le W$) and W the layer width. The maximal damping $\nu_{\max}$ is proportional to a predefined nominal frequency. Thus, the layer width required to absorb acoustical waves is proportional to the wavelength λ.

The damping layer with the above properties was implemented and tested using one-dimensional planar waves with different frequencies and layer widths without mean flow. The reflection coefficient R of the layer was evaluated and the results are displayed in Figure 5. As it is seen, while locally minimal reflectivity can be achieved for a monochromatic wave using smaller layer widths as well, to arrive at small reflectivity in a broad range of frequencies a wide layer is required and the width should be chosen based on the minimal frequency.

The effect of reflections from the inlet were finally suppressed to a sufficient extent by adding a damping layer of 6 m width at the top of the simulation domain. The damping layer contained $\approx$ 30 000 additional elements. A similar solution was applied previously in cavity tone simulations [6].

Flow-induced resonance

The excitation of the resonator by grazing flow was simulated at different flow speeds. At low flow speeds ($U \approx 6\,\mathrm{m/s}$) an interesting phenomenon was observable in the pressure and velocity probe data. In these cases, two hydrodynamic modes of the shear layer can be excited. However, the two modes do not exist at the same time, rather, mode switching occurs, as also observed in the measurements [1]. The phenomenon is illustrated in Figure 6, where the spectrogram of the pressure fluctuations at the center of the bottom of the resonator is shown. As seen, at around $t \approx 0.9\,\mathrm{s}$ the oscillation of the first hydrodynamic mode dies out and the second mode becomes dominant, while at $t \approx 1.3\,\mathrm{s}$ the reverse process takes place. The effect is also visible looking at the third harmonic of the first mode with $3f_1 \approx 70\,\mathrm{Hz}$. It is also observed that the frequency of the second mode is not exactly twice that of the first mode, contrary to the expectations from eq. (1). This is in good correspondence with the measurements and simulations in [1] and [3].

Figure 7 shows the amplitude spectra of pressure fluctuations at the bottom center position of the resonator at three different flow speeds. As seen, when the oscillation frequency of the shear layer is close to the natural resonance frequency of the Helmholtz resonator ($U \approx 15\,\mathrm{m/s}$ here), strong acosutical resonance occurs. In this case, narrow harmonic peaks are observed in the spectrum indicating a purely periodic response. If the freestream

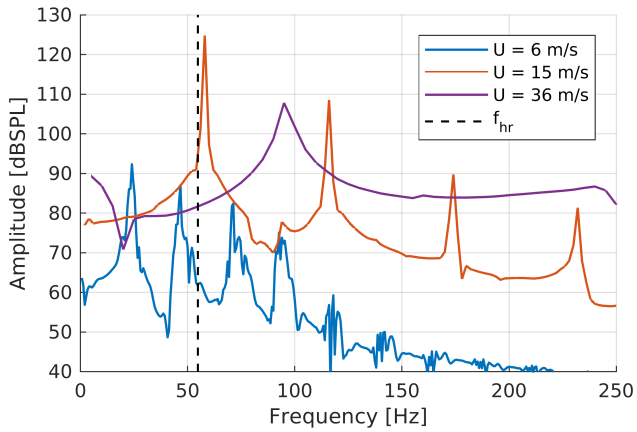

Figure 7: Amplitude spectra of the fluctuating pressure at the bottom of the resonator at different flow speeds.

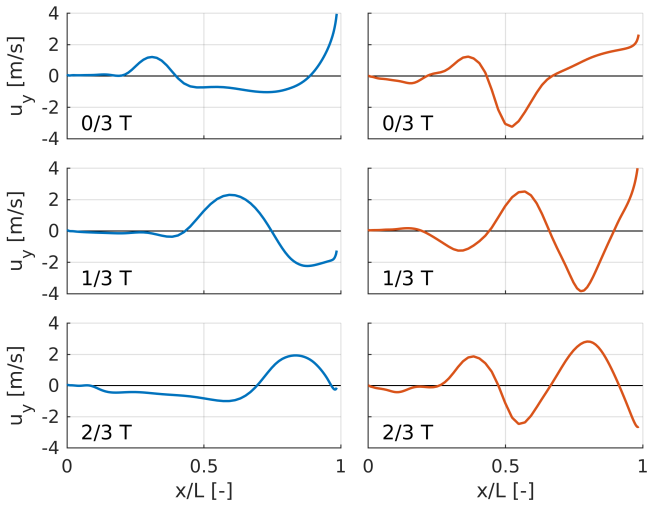

Figure 8: Comparison of the shear layer oscillations without (left) and with (right) acoustical feedback at $U = 15\,\mathrm{m/s}$.

velocity is further increased and the shear layer oscillation frequency becomes much higher than f_{hr}, the amplitude of the osciallation diminishes and the broadband components of the response become more dominant. In case of $U = 36\,\mathrm{m/s}$ the peak at $f \approx 90\,\mathrm{Hz}$ appears due to the non-physical acoustical reflections from the inlet, as discussed above. The velocity dependent behavior of the pressure spectrum is in agreement with that reported in [1] and [3].

An observed discrepancy between previous investigations [1, 3] and the simulation results presented here, is that the relative amplitude of the second harmonic is 10–15 dB higher in the simulations using the 2D model, while the relative amplitudes of higher harmonics show a good correspondence. Another observation not discussed in the references is that at higher flow speeds ($U > 30\,\mathrm{m/s}$) the transverse acoustical mode of the resonator with the eigenfrequency $f_{\mathrm{tr}} \approx 345\,\mathrm{Hz}$ is also efficiently excited by the harmonics of the shear layer oscillation frequency.

Figure 8 shows a comparison of the cross-stream velocities without and with acoustical feedback at different time instances in one period of the shear layer oscillations. As it is seen, the acoustical resonance has a strong feedback effect on the shear layer. The amplitude of the cross-stream velocity is significantly increased, especially near the middle of the orifice. In both cases vortex generation yields a large velocity gradient at the trailing edge.

Conclusions and outlook

This paper presented a simulation study of a flow-excited Helmholtz resonator. Compared to previous examinations, the shear layer oscillations and the acoustical response of the resonator were also simulated separately beside considering flow-induced resonance. This approach enables quantifying the strength of acoustical feedback on the shear layer oscillations.

A shortcoming of the 2D model presented here is the limited choice of available turbulence modeling strategies. As future work, 3D geometries will also be studied and LES will be used. Finally, in order to separate flow and acoustical oscillations, the applicability of flow field decomposition methods is to be explored.

Acknowledgments

The author gratefully acknowledges the support of the Bolyai János research grant provided by the Hungarian National Academy of Sciences.

Supported by the ÚNKP-18-4 New National Excellence Program of the Ministry of Human Capacities.

References

[1] R. Ma, P. E. Slaboch, and S. C. Morris. Fluid mechanics of the flow-excited Helmholtz resonator. *Journal of Fluid Mechanics*, 623:1–26, 2009.

[2] X. Dai, X. Jing, and X. Sun. Flow-exciated acoustic resonance of a Helmholtz resonator: Discrete vortex model compared to experiments. *Physics of Fluids*, 27:057102–1–24, 2015.

[3] F. Ghanadi, M. Arjomandi, B. Cazzolato, and A. Zander. Understanding of the flow behaviour on a Helmholtz resonator excited by grazing flow. *International Journal of Computational Fluid Dynamics*, 28(5):1–13, 2014.

[4] OpenCFD release OpenFOAM v1812. `https://www.openfoam.com/releases/openfoam-v1812/` Last visited: March 28, 2019.

[5] C. A. Wagner, T. Hüttl, and P. Sagaut, editors. *Large-eddy simulation for acoustics*. Cambridge University Press, 2007.

[6] P. T. Nagy, A. Hüppe, M. Kaltenbacher, and Gy. Paál. Aeroacoustic simulations of the cavity tone. In *Conference on Modelling Fluid Flow (CMFF '15)*, pages *–8, 2015.